Chinese Chemical Letters 31 (2020) 1680–1685

Contents lists available at ScienceDirect

Chinese Chemical Letters

journal homepage: www.elsevier.com/locate/cclet

Communication

Solution-phase synthesis of ordered mesoporous carbon as resonant-gravimetric sensing material for room-temperature H_2S detection

Jiawei Ni[a,1], Tao Zhao[a,1], Lei Tang[b,c], Pengpeng Qiu[a], Wan Jiang[a], Lianjun Wang[a], Pengcheng Xu[b,d,**], Wei Luo[a,*]

[a] State Key Laboratory for Modification of Chemical Fibers and Polymer Materials, College of Materials Science and Engineering, Institute of Functional Materials, Donghua University, Shanghai 201620, China
[b] State Key Laboratory of Transducer Technology, Shanghai Institute of Microsystem and Information Technology, Chinese Academy of Sciences, Shanghai 200050, China
[c] College of Life and Environmental Sciences, Shanghai Normal University, Shanghai 200234, China
[d] University of Chinese Academy of Sciences, Beijing 100049, China

ARTICLE INFO

Article history:
Received 2 October 2019
Received in revised form 6 November 2019
Accepted 15 November 2019
Available online 16 November 2019

Keywords:
Mesoporous materials
Carbon
Self-assembly
Resonant cantilever gas sensor
H_2S

ABSTRACT

H_2S can cause multiple diseases and poses a great threat to human health. However, the precise detection of extremely toxic H_2S at room temperature is still a great challenge. Here, a facile solvent evaporation induced aggregating assembly (EIAA) method has been applied for the production of ordered mesoporous carbon (OMCs) in an acidic THF/H_2O solution with high-molecular-weight poly(ethylene oxide)-*b*-polystyrene (PEO-*b*-PS) copolymers as the structure-directing agent, formaldehyde and resorcinol as carbon precursors. Along with the continuous evaporation of THF from the mixed solution, cylindrical micelles are formed in the solution and further assemble into highly ordered mesostructure. The obtained OMCs possesses a two-dimensional (2D) hexagonal mesostructure with uniform and large pore diameter (~19.2 nm), high surface area (599 m^2/g), and large pore volume (0.92 cm^3/g). When being used as the resonant cantilever gas sensor for room-temperature H_2S detection, the OMCs has delivered not only a superior gas sensing performance with ultrafast response (14 s) and recovery (21 s) even at low concentration (2 ppm) but also an excellent selectivity toward H_2S among various common interfering gases. Moreover, the limit of detection is better than 0.2 ppm, indicating its potential application in environmental monitoring and health protection.

Hydrogen sulfide (H_2S) is a highly toxic, corrosive and flammable gas with a rotten egg-like smell, which is usually originated from natural gas exploration, oil and gas industries, sewage treatment, automobile exhaust gas, as well as the decomposition of organic compounds [1–4]. Exposure to a low concentration of H_2S may lead to critical health problems such as nose and eye irritation, olfactory nerve paralysis. At a high concentration (100 ppm), H_2S gas may lead an immediate collapse with loss of breathing and a high death probability [2,5]. In addition, H_2S is also responsible for the causation of some diseases such as Down syn-drome, Parkinson's disease, Alzheimer's disease, *etc.* [5,6]. Therefore, precision detection and monitoring of trace H_2S (ppm or sub-ppm level) at ambient atmosphere is highly crucial and desirable [1,7,8]. Up to now, bulky instruments such as gas chromatography-mass spectrometry (GC–MS) and high-performance liquid chromatography (HPLC) are generally used to detect H_2S with high-accuracy [1,8]. However, these methods are tedious, labor-intensive and expensive. Compared with the above-mentioned instruments, semiconductor-based resistive gas sensors have been considered as appealing candidates due to the merits of remarkable sensitivity, small volume, low cost and on spot operation [9–12]. The sensing mechanism of semiconductor-based sensors is widely considered to be the change in conductivity when exposed in specific gas, the adsorbed gas molecules may cause increase/decrease in the resistance of

* Corresponding author.
** Corresponding author at: State Key Laboratory of Transducer Technology, Shanghai Institute of Microsystem and Information Technology, Chinese Academy of Sciences, Shanghai 200050, China.
E-mail addresses: xpc@mail.sim.ac.cn (P. Xu), wluo@dhu.edu.cn (W. Luo).
[1] These authors contributed equally to this work.

https://doi.org/10.1016/j.cclet.2019.11.025

semiconductors [13–17]. Among diverse semiconducting sensing materials, semiconducting metal oxides (SMOs, such as WO_3, ZnO, In_2O_3 and SnO_2) have been demonstrated as promising candidates for H_2S sensing due to high sensitivity, fast response/recovery speed and excellent stability [2,18,19]. However, the working temperature of SMOs-based sensors was usually high (150−400 °C) for enhanced sensing performance, which significantly increases the energy consumption and the cost of gas sensors [18–22]. In addition, heating up to high temperature may also lead to the collapse of rational designed microstructure, which is resulting in degradation of sensing performance [23]. Therefore, it is highly desired to develop H_2S gas sensors operated at room temperature, in order to enhance the device stability, as well as minimize the energy consumption and cost.

As a kind of mass-type transducer, resonant microcantilever transforms adsorption induced mass-change into frequency-shift sensing signal, which has drawn intensive attention because of the ultra-high sensitivity, high stability and miniaturized device size [24–26]. More importantly, the working temperature of resonant cantilever gas sensor was greatly reduced compared to semiconductor-based resistive gas sensors [27]. According to the working mechanism of resonant microcantilevers, the development of sensing materials with interconnected pore structure and abundant active sites is of great importance to enhance the sensing performance [28]. As an important kind of porous materials, ordered mesoporous carbon (OMCs) has some extensive advantages such as high surface areas, ordered pore arrangement, hierarchical pore structure and abundant natural sources [29–38], which can provide numerous active sites for interaction with H_2S vapor and facilitate the rapid and effective diffusion of gas molecules. Therefore, OMCs is regarded as promising candidates for resonant microcantilevers gas sensing materials. To date, various OMCs were fabricated with different mesostructures and morphologies [39–44]. However, most of the synthetic routes were based on the tedious solvent evaporation induced self-assembly (EISA) approach by using commercially available surfactants (such as Pluronic P123, F127) [45–50], which is not favorable for large scale synthesis and precise control of pore sizes as well as wall thickness. Consequently, it is of great importance to explore facile and controllable approaches in solution phase to fabricate OMCs with well-defined mesostructures to achieve excellent sensing performance.

Herein, we have developed a simple and facile solvent evaporation induced aggregating assembly (EIAA) strategy to synthesize OMCs with uniform and large pore sizes, two-dimensional (2D) hexagonal mesostructure and excellent pore interconnectivity, in which laboratory-made water insoluble block copolymer PEO-*b*-PS as template, formaldehyde and resorcinol as carbon precursors, acidic mixture of tetrahydrofuran (THF) and H_2O as reaction medium. In this approach, ordered mesostructure was self-assembled at the liquid (THF)-liquid (H_2O) interface with the selective evaporation of the THF solvent from THF-rich solution. The obtained mesostructured composites were carbonized by pyrolysis treatment in N_2 atmosphere, resulting in OMCs with uniform and large mesopore size (19.2 nm), high surface area (599 m^2/g) and large pore volume (0.92 cm^3/g). More importantly, the resultant OMCs was used to fabricate a resonant cantilever gas sensor which can work at room temperature and exhibit significantly excellent H_2S gas sensing performance with fast response (14 s) and recovery (21 s), ultralow limit of detection of 0.2 ppm, as well as good selectivity, which contributes to their good merits of unique porous structure and numerous active sites. Such a good performance making them be an excellent candidate as high-performance gas sensors. This facile EIAA approach opens up new horizons for synthesis of highly ordered mesoporous materials with different frameworks.

Monomethyl poly(ethylene oxide) (Mw: 5000 g/mol, designed as PEO5000), 2-bromoisobutyryl bromide, copper(I) bromide were purchased from Sigma-Aldrich. *N*,*N*,*N*′,*N*′,*N*″-pentamethyl diethylenetriamine (PMDETA) was purchased from Arcos. Tetrahydrofuran (THF), Pyridine, ethanol, styrene, anhydrous ethyl ether, petroleum ether (30 − 60 °C), Al_2O_3, resorcinol, formaldehyde aqueous solution (37 wt%) and hydrochloric acid were purchased from Sino-Pharm Chemical Reagent Co., Ltd. Chemicals and solvents in analytical grade were purchased and used as received.

OMCs were prepared through the EIAA approach by using amphiphilic diblock copolymer PEO-*b*-PS as the structure directing agent. In a typical synthesis, PEO-*b*-PS with high molecular weight was prepared *via* atom transfer radical polymerization (ATRP) approach according to our previous work [51]. This template has a molecular composition of PEO_{114}-*b*-PS_{199} with narrow molecular weight distribution (polydispersity index, PDI = 1.13) according to gel permeation chromatography (GPC) and 1H-NMR. In a typical synthesis of OMCs, PEO-*b*-PS template (45 mg) was first dissolved in THF (15.0 mL) and water (2.0 mL) to form clear solution in a glass vial under stirring. Meanwhile, resorcinol (0.10 g) was dropwise added into the above transparent solution under continuous magnetic stirring. After that, the solution was left to stand for evaporation of THF at room temperature in air in a hood under continuous stirring. After stirring at room temperature for 3 h, formaldehyde aqueous solution (0.14 mL) and hydrochloric acid (0.02 mL) were added. The reaction was allowed to proceed under stirring until the THF solvent was completely evaporated. After 30−40 h, red PEO-*b*-PS/Resorcinol-formaldehyde (RF) composite product were precipitated from the solution and collected by centrifugation, followed by washed with water for three times and dried in an over at 60 °C. Finally, the OMCs with 2D hexagonal mesostructure and large pore size were obtained after annealing under nitrogen at 600 °C for 3 h to remove PEO-*b*-PS template.

Transmission electron microscopy (TEM) measurements were carried out on a JEOL 2100 microscope (Japan) operated at 200 kV. Field-emission scanning electron microscopy (FESEM) images were obtained on the Hitachi model S-4800 field emission scanning microscope. Nitrogen adsorption-desorption isotherms were measured at 77 K with a Micromeritics Tristar 3020 analyzer. Before measurement, the samples were degassed under vacuum at 180 °C for at least 6 h. The specific surface area was calculated using the Brunauer-Emmett-Teller (BET) method using the adsorption data in a relative pressure (P/P_0) range from 0.005 to 0.25. The pore volume and pore size distribution were calculated by using the Barrett-Joyner-Halenda (BJH) model from the adsorption branches of isotherms. The total pore volumes (V) were estimated according to the adsorbed amount at a relative pressure P/P_0 of 0.995. Raman spectra were recorded using micro-Raman spectroscopy (Renishaw inVia Reflex, excited by 633 nm He-Ne red laser, Britain). X-ray photoelectron spectroscopy (XPS, PHI-5000C ESCA) was collected with Mg Kα radiation ($h\nu$ =1253.6 eV) and Al Kα radiation ($h\nu$ = 1486.6 eV). All of the binding energy values were charge corrected to the adventitious carbon (C 1s = 284.6 eV).

OMCs material (10 mg) was dispersed into deionized water (1.0 mL) to form a crude suspension under ultrasonic treatment, which was used as ink in the following material deposition experiment. Then, several drops of the obtained ink were printed on the top-surface of microcantilever by using a commercial GIX II Microplotter (Sonoplot Inc.). After that, the microcantilever was dried in an oven at 60 °C for 2 h. For sensing performances measurement, the as-fabricated sensor was put into a home-made testing chamber (20 L). And a commercial frequency counter (Agilent, model 53131A) was connected to the cantilever sensor for date acquisition. Before gas sensing, the frequency value of cantilever sensor is recorded as baseline signal. After that, certain concentration H_2S was diluted by injecting certain volume gas into

the testing chamber with known volume of 20 L. After one-cycle gas detection, the testing chamber was switching opened to clean air atmosphere. The above-mentioned measurements were conducted under air atmosphere and room temperature (25 °C). The sensing response was denoted as Δf (the frequency change of sensors before and after exposing to target gases).

Amphiphilic diblock copolymer PEO_{114}-*b*-PS_{199} (molecular weight 25636 g/mol, polydispersity index 1.13) was synthesized *via* an atom transfer radical polymerization (ATRP) approach. Because of the hydrophobic property of PS segments, PEO-*b*-PS template was first dissolved in the mix solution with a high ratio of THF solvent, which is a good solvent for both PEO and PS segments. Fig. 1 presents the EIAA process for the ordered mesoporous carbon starting from THF/H_2O solution containing the block copolymer template. With the continuous evaporation of THF at room temperature, the solvency power of the solution for block copolymer template decreased sharply because water is the poor solvent for PS segments, and the good solvent for PEO segments. It induces the copolymer self-assemble into cylindrical micelles with PS block as core surrounded by PEO shells under stirring. After adding resorcinol, the resorcinol species can interact with PEO segment *via* hydrogen bonds to form cylindrical composite micelles. Then, formaldehyde and hydrochloric acid was introduced, forming cylindrical core-shell micelles with rod-like PS microdomains covered by PEO/Resorcinol-formaldehyde (RF) resin composites after the polymerization of resorcinol and formaldehyde. With the continuous evaporation of THF, highly ordered 2D mesoporous structure was obtained due to the balance of repulsion force of negatively charged rods and the van der Waals attraction force (Step 1). As a result, reddish precipitate could be separated from the solution phase. Such ordered mesostructure can be subsequently solidified by thermal treatment at 60 °C to increase cross-linking degree of RF polymer (Step 2). Finally, the OMCs with 2D hexagonal mesostructure and large pore size were obtained after pyrolysis under nitrogen at 600 °C for 3 h to remove PEO-*b*-PS template (Step 3) [52].

The small-angle X-ray scattering (SAXS) pattern of the as-made RF/PEO-*b*-PS composites shows weak scattering peaks (Fig. 2a-1), it can be attributed to the inadequate mass contrast of organic-organic frameworks. After pyrolysis at 600 °C under N_2 atmosphere, the obtained OMCs displays three well-resolved peaks at *q* value of 0.213, 0.541, 0.825 nm^{-1} (Fig. 2a-2). These peaks can be indexed as the 100, 110 and 200 reflections of ordered 2D hexagonal mesostructure with the space group *p6mm*, implying that the ordered mesostructure is well retained after calcination. The unit-cell parameter (a_0) is calculated to be as large as 34.1 nm, indicative of the large unit of mesostructure. Field emission scanning electron spectroscopy (FESEM) observations of OMCs after calcination at 600 °C in an inert atmosphere show highly ordered 2D hexagonal arrays of mesopores over a large domain viewed from [100] (Fig. 3a) and [110] (Fig. 3b) directions, which attribute to the removal of amphiphilic diblock copolymer PEO-*b*-PS template. The diameter of mesopore is roughly estimated to be about 21.0 nm from the FESEM image, indicating a large pore size. The inset image in Fig. 3a indicates regular columnar channel section. The transmission electron microscopy (TEM) images of the OMCs taken from the [100] (Fig. 3c) and [110] (Fig. 3d) directions further reveal its well-defined 2D hexagonal (*p6mm*) symmetry with a remarkably high regularity, which shows both mesopores and tubular channels. The mesopore size is measured to be about 22.0 nm, which is well matched with the SEM observations. Furthermore, the cell parameter of OMCs sample is estimated from the TEM image to be ~32.0 nm, in good agreement with the value calculated from SAXS information. The above-mentioned results show that ordered mesostructure was formed *via* the EISA process of PEO-*b*-PS template with polymer (RF) species into cylindrical micelles. And highly ordered OMCs was obtained after thermal treatment process, indicating a good thermal stability.

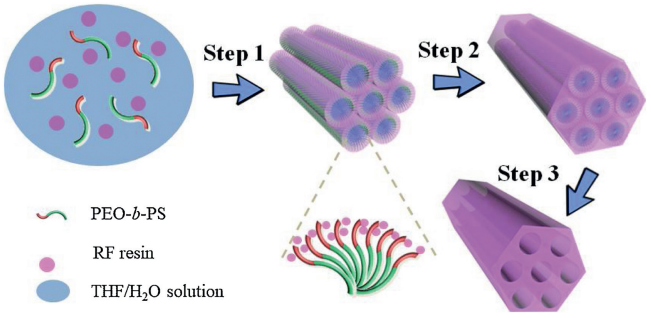

Fig. 1. Schematic illustration for the synthesis of OMCs *via* EIAA approach strategy. Step 1: The co-assembly of PEO-*b*-PS and RF resin into cylindrical micelles as THF solution evaporates, and the cylindrical nanocomposites further assemble into an ordered *p6mm* mesostructure. Step 2: The composite micelles precipitate from the residual solution, and thermosetting in oven at 60 °C for further solidification. Step 3: Pyrolysis of the composites with 2D hexagonal mesostructure under N_2 atmosphere at 600 °C, resulting in OMCs with uniform pore sizes.

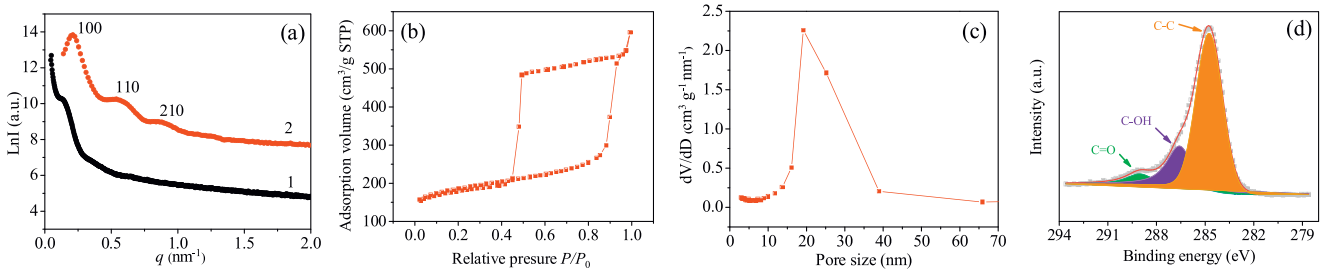

Fig. 2. (a) SAXS patterns of the (1) as-made RF/PEO-*b*-PS composites and (2) OMCs obtained after pyrolysis at 600 °C, patterns are vertically offset for clarity. (b) Nitrogen adsorption–desorption isotherm and (c) the corresponding pore size distribution curve of the obtained OMCs. (d) XPS spectra of the obtained OMCs in the vicinity of C 1s.

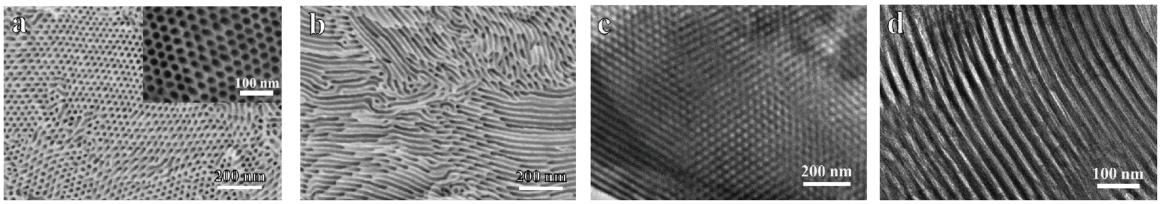

Fig. 3. FESEM (a, b) and TEM (c, d) images of OMCs obtained after pyrolysis at 600 °C taken along the directions of [100] (a, c) and [110] (b, d).

The N_2 adsorption–desorption isotherms of the OMCs after pyrolysis at 600 °C in N_2 show characteristic type IV curves with H1 hysteresis loop with a distinct capillary condensation step at relative pressure (P/P_0) of 0.84-0.93 (Fig. 2b), indicating a highly uniform 2D hexagonal mesostructure with large pore size. The pore size distribution profiles derived from the adsorption branch of the isotherms calculated by using Barrett-Joyner-Halenda (BJH) model indicates that the OMCs has a large and uniform pore size of 19.2 nm (Fig. 2c), mainly due to the removal of large hydrophobic PS segments in PEO-*b*-PS template. Taking the cell parameter of OMCs (a_0 = 34.1 nm) derived from SAXS data into account, the pore wall thickness of OMCs is calculated to be about 14.9 nm. The specific surface area and total pore volume of the OMCs are calculated to be 599 m^2/g and 0.92 m^3/g, respectively. The well-connected mesoporous structure with large pore sizes and high specific surface areas could greatly facilitate the diffusion of gas molecules and provide abundant active sites, which makes OMCs promising candidates for gas sensing, energy storage and conversion, as well as catalysis. More detailed information on the chemical state of the elements was obtained from the X-ray photoelectron spectroscopy (XPS) measurement. The XPS spectrum of C 1s region consists of three peaks centering at 284.8 eV, 286.6 eV, and 289.1 eV (Fig. 2d), which can be ascribed to graphitic carbon (C—C), C in C—OH and C in C=O, respectively. The XPS spectrum of O 1s region consists of three peaks centering at 533.8 eV, 535 eV and 536.6 eV (Fig. S2 in Supporting information), which can be ascribed to C—O, O adsorbed on the surface, and O in C=O, respectively. Oxygen atoms contribute to better adsorption of H_2S [53]. Raman spectroscopy can be used to characterize G and D bands of the obtained OMCs, and the intensity ratio of D band to G band (I_D/I_G) is usually recognized to reflect the defects and disorder degree of the graphitized structure. The Raman spectra of OMCs in Fig. S1 (Supporting information) display the D band at 1350 cm^{-1} and G band at 1598 cm^{-1}, respectively. The intensity ratio (I_D/I_G) for this sample is 0.80, which represents a high degree of graphitization.

Up to now, very few work synthesized OMCs with large pores in acid solution phase, which are beneficial for mass production and desirable in practical applications. Consequently, the development of our facile and simple solution phase synthesis strategies is of great importance. Such accurately designed synthetic strategy also pave a new way toward the construction of ordered mesoporous materials with diverse frameworks. In addition, encouraged by the unique structure of the obtained OMCs such as efficient gas diffusion channel, highly ordered and interconnected pore structure, high specific surface area, we further fabricated OMCs-based H_2S gas sensing sensors to investigate their potential application in gas detection field. In this work, inkjet printing method was applied in the laboratory to fabricate OMCs-based resonant microcantilever H_2S gas sensor. SEM image of the as-prepared mass-type sensor in Fig. 4a clearly indicated that OMCs was precisely loaded onto its free-end.

The fabricated sensor was put inside a chamber for gas sensing measurements at room temperature (25 °C). For H_2S gas sensing

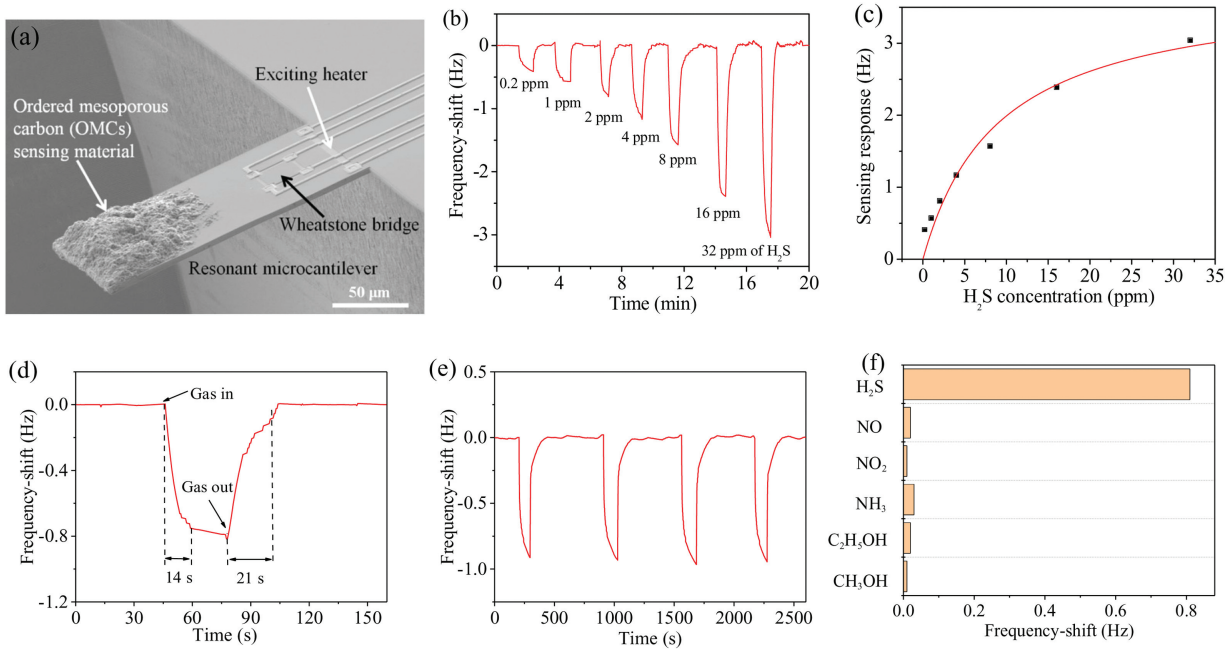

Fig. 4. (a) SEM image of the resonant microcantilever sensor, where the OMCs sensing material is inkjet deposited onto the free-end of the cantilever. (b) Resonant-gravimetric sensing curve of the obtained OMCs to H_2S of various (0.2~32 ppm) concentrations. (c) Relationship between H_2S concentration and sensing response, which can be well fitted as a function of the Langmuir equation. (d) Resonant-gravimetric sensing curve of the obtained OMCs to 2 ppm H_2S. (e) Repeatable detection of the sensor to H_2S with identical concentration of 3 ppm. (f) Selectivity of the as-fabricated resonant-gravimetric sensor to H_2S and various interfering gases with identical 2 ppm concentration.

measurements, H_2S-contained gas was injected into the test chamber at room temperature while the mass addition (Δm) of OMCs material was real-time measured, attribute to H_2S adsorption. It should be noted that Δm leads the frequency-shift (Δf) of the sensor drops proportionally due to the relationship of $\Delta f \propto \Delta m$. The H_2S sensing performance of the OMCs based microcantilever sensor was measured and summarized in Fig. 4. The typical sensor response curve in Fig. 4b displays frequency change of the sensor toward H_2S concentrations in the range of 200 ppb to 32 ppm. Each sensing cycle for specific concentration was completed within 2 min, exhibiting both fast response and quick recovery of the sensor. As shown in Fig. 4b, with the increase of H_2S concentration, the response values of the OMCs-based sensor increased accordingly. In addition, the sensor outputs a response (Δf) of 0.42 Hz to 200 ppb of H_2S, which is 16 times higher than the noise level of ±0.025 Hz. Obviously, the experimentally observed limit of detection (LOD) of the sensor in this study is much better than 200 ppb. The performance of mesoporous carbon FDU-15 templated from Pluronic copolymers under the same conditions is shown in Fig. S3 (Supporting information). The response values are much lower than our OMCs, showing poor sensitivity, may attribute to the smaller pore size. As shown in Fig. 4c, the relationship between Δf and H_2S concentration that is derived from the above-mentioned sensing curve can be well fitted with Langmuir theory and the Langmuir equation is $S = 0.4169C/(1 + 0.11C)$, where S and C respectively denote sensing response and H_2S concentration.

The response and recovery behaviors are crucial to evaluate the sensing performance of materials. The response time is defined as the time required from initial state to 90% of the maximum response after the sensor exposed to H_2S gas, and the recovery time is defined as 90% of the total time required from maximum response to baseline, respectively. The OMCs based sensor exhibits a fast response of 14 s upon exposure to 2 ppm H_2S and quick recovery of 21 s when H_2S gas was removed (Fig. 4d). Moreover, the repeatability of the OMCs-based sensor to H_2S is also investigated. As shown in Fig. 4e, the detection to 3 ppm H_2S are repeated for 4 times. The frequency-drop (Δf) values of the sensor are obtained as 0.91 Hz, 0.93 Hz, 0.96 Hz and 0.95 Hz, respectively. The relative standard deviation (RSD) is calculated to be 1.9%, which represents a good repeatable detection capability. These results indicate that our OMCs-based sensor exhibits very competitive performance compared with the previously reported H_2S sensors [53–67] (Table S1 in Supporting information), including high sensitivity, satisfied detection limit, as well as ultrafast response and recovery speed. Notably, all of the above-mentioned good sensing properties are achieved at room temperature, which can significantly increase sensor stability and lifetime, as well as reduce the cost of gas sensor. The satisfied sensing properties of the OMCs-based sensor are attributed as follows: (1) The high specific surface area of OMCs can provide abundant active sites in the solid-gas interfaces, which greatly facilitate the adsorption of a large amount of H_2S molecules; (2) The uniform, large and well-connected mesopores are able to efficiently boost the mass transfer during the sensing process. Therefore, it can be concluded that the unique nanostructure of our OMCs could maximize the comprehensive sensing performance, which might have great potential for environmental monitoring and health protection. The selectivity is also a crucial parameter of gas sensors for their practical application. In this work, the responses of OMCs-based sensor to multiple interfering gas sources (2 ppm), including nitrogen monoxide, nitrogen dioxide, ammonia, ethanol, methanol were measured for comparison with H_2S gas (2 ppm) at room temperature. As shown in Fig. 4f, our OMCs-based sensor displays much higher response to H_2S than that of the selected interfering gases, thus showing promising potential for practical applications. The good selectivity of our OMCs-based sensor to H_2S target gas can be attributed to the strong and specific interaction between porous carbon and H_2S molecules as reported in literatures [68–70].

In summary, we have developed a facile and novel EIAA approach for the construction of OMCs with 2D hexagonal pore arrangement, improved pore connectivity and uniform pore size. It was accomplished in the acidic THF/H_2O mixture by using high molecular-weight PEO-*b*-PS copolymers as a template, formaldehyde and resorcinol as carbon precursors. The continuous evaporation of THF in this system is critical, which can enable the self-assembly on the THF-H_2O interface. The specific surface areas, pore diameter and pore volume of as-prepared OMCs are as high as 599 m^2/g, 19.2 nm and 0.92 cm^3/g. The interconnected mesoporous structure and abundant active sites endow the obtained OMCs-based sensor with fast response (14 s) and recovery (21 s) dynamics, ultra-high sensitivity (0.2 ppm), as well as excellent selectivity for H_2S sensing at room temperature. Based on the above-mentioned results, the as-prepared OMCs hold a great promise for development of high-performance gas sensors for various applications such as environmental monitoring and health protection. Furthermore, this simple but versatile EIAA strategy is expected to be extended to fabricate highly ordered mesoporous materials with various skeleton composition.

Declaration of competing interest

The authors declare that they have no known competing financial interests or personal relationships that could have appeared to influence the work reported in this paper.

Acknowledgments

This research is supported by the National Natural Science Foundation of China (Nos. 51822202 and 51772050), Shanghai Rising-Star Program (No. 18QA1400100), Youth Top-notch Talent Support Program of Shanghai, the Shanghai Committee of Science and Technology, China (No. 19520713200), Key Research Program of Frontier Sciences of Chinese Academy of Sciences (No. QYZDJ-SSW-JSC001), DHU Distinguished Young Professor Program and Fundamental Research Funds for the Central Universities. P. Xu appreciates the financial support of the Youth Innovation Promotion Association CAS (No. 2016213).

Appendix A. Supplementary data

Supplementary material related to this article can be found, in the online version, at doi:https://doi.org/10.1016/j.cclet.2019.11.025.

References

[1] Y.H. Li, W. Luo, N. Qin, et al., Angew. Chem. Int. Ed. 53 (2014) 9035–9040.
[2] A. Mirzaei, S.S. Kim, H.W. Kim, et al., J. Hazard. Mater. 357 (2018) 314–331.
[3] S. Moon, N.M. Vuong, Lee D, et al., Sens. Actuator. B: Chem. 222 (2016) 166–172.
[4] H. Tajizadegan, M. Rashidzadeh, M. Jafari, et al., Chin. Chem. Lett. 24 (2013) 167–169.
[5] M.A.H. Khan, M.V. Rao, Q. Li, et al., Sensors 19 (2019) 905.
[6] J. Zhang, R. Sokolovvskij, G.H. Chen, et al., Sens. Actuator. B: Chem. 280 (2019) 138–143.
[7] H.R. Zhang, L.Y. Niu, Y.Z. Chen, et al., Chin. Chem. Lett. 27 (2016) 1793–1796.
[8] Y.H. Li, X.R. Zhou, W. Luo, et al., Adv. Mater. Interfaces 6 (2019) 1801269.
[9] W.C. Wang, F.Q. Liu, B. Wang, et al., Chin. Chem. Lett. 30 (2018) 1261–1265.
[10] X.R. Zhou, X.W. Cheng, Y.H. Zhu, et al., Chin. Chem. Lett. 29 (2018) 405–416.
[11] Y.H. Zhu, Y. Zhao, J.H. Ma, et al., J. Am. Chem. Soc. 139 (2017) 10365–10373.
[12] X.Y. Xiao, X.R. Zhou, J.H. Ma, et al., ACS Appl. Mater. Interfaces 11 (2019) 26268–26276.
[13] G. Wang, J. Qin, X.R. Zhou, et al., Adv. Funct. Mater. 28 (2018) 1806144.
[14] J.H. Hao, Y. Ren, X.R. Zhou, et al., Adv. Funct. Mater. 28 (2018) 1705268.
[15] Y. Ren, X.R. Zhou, W. Luo, et al., Chem. Mater. 28 (2016) 7997–8005.
[16] Y. Zhang, Y.Y. Fu, D.F. Zhu, et al., Chin. Chem. Lett. 27 (2016) 1429–1436.

[17] J.Q. Xu, Z.G. Xue, N. Qin, et al., Sens. Actuator B: Chem. 242 (2017) 148–157.
[18] F.I.M. Ali, F. Awwad, Y.E. Greish, et al., IEEE Sens. J. 19 (2019) 2394–2407.
[19] C. Li, Z.S. Yu, S.M. Fang, et al., Chin. Chem. Lett. 19 (2008) 599–603.
[20] Z.R. Wang, Y.H. Zhu, W. Luo, et al., Chem. Mater. 28 (2016) 7773–7780.
[21] Y.D. Zou, X.R. Zhou, Y.H. Zhu, et al., Acc. Chem. Res. 52 (2019) 714–725.
[22] Y. Ren, X.Y. Yang, X.R. Zhou, et al., Chin. Chem. Lett. 30 (2019) 2003–2008.
[23] Z.J. Li, H. Li, Z.L. Wu, et al., Mater. Horiz. 6 (2019) 470–506.
[24] Y.Q. Lv, H.T. Yu, P.C. Xu, et al., Sens. Actuator. B: Chem. 256 (2017) 639–647.
[25] T. Xu, P.C. Xu, D. Zheng, et al., Anal. Chem. 88 (2016) 12234–12240.
[26] I. Dufour, S.M. Heinrich, F. Josse, Proc. 2004 IEEE Intern. 16 (2007) 44–49.
[27] S.B. Guo, P.C. Xu, H.T. Yu, et al., Sens. Actuator B: Chem. 209 (2015) 943–950.
[28] S.R. Cai, W. Li, P.C. Xu, et al., Analyst 144 (2019) 3729–3735.
[29] L. Peng, C.T. Hung, S.W. Wang, et al., J. Am. Chem. Soc. 141 (2019) 7073–7080.
[30] J. Zhang, J. Wang, Z.Q. Shi, et al., Chin. Chem. Lett. 29 (2018) 80–83.
[31] H.B. Zhang, P.F. An, W. Zhou, et al., Sci. Adv. 4 (2018) eaao6657.
[32] F.L. Meng, Z.L. Wang, H.X. Zhong, et al., Adv. Mater. 28 (2016) 7948–7955.
[33] H.W. Zhang, O. Noonan, X.D. Huang, et al., ACS Nano 10 (2016) 4579–4586.
[34] W.H. Li, Z.Z. Yang, M. Li, et al., Nano Lett. 16 (2016) 1546–1553.
[35] J. Tang, J. Liu, C.L. Li, et al., Angew. Chem. Int. Ed. 54 (2015) 588–593.
[36] Z.Y. Guo, D.D. Zhou, X.L. Dong, et al., Adv. Mater. 25 (2013) 5668.
[37] J. Schuster, G. He, B. Mandlmeier, et al., Angew. Chem. Int. Ed. 51 (2012) 3591–3595.
[38] B.K. Guo, X.Q. Wang, P.F. Lulvio, et al., Adv. Mater. 23 (2011) 4661.
[39] Q. Shi, R.Y. Zhang, Y.Y. Lu, et al., Carbon 84 (2015) 335–346.
[40] Y. Fang, Y.Y. Lv, F. Gong, et al., Adv. Mater. 28 (2016) 9385.
[41] R.L. Liu, L. Wan, S.Q. Liu, et al., Adv. Funct. Mater. 25 (2015) 526–533.
[42] S. Li, C. Cheng, A. Sagaltchik, et al., Adv. Funct. Mater. 29 (2019) 1807419.
[43] M. Zhang, L. He, T. Shi, et al., Chem. Mater. 30 (2018) 7391–7412.
[44] Y. Liu, Z.R. Wang, W. Teng, et al., J. Mater. Chem. A 6 (2018) 3162–3170.
[45] H. Xie, Y.J. Zhao, Y. Tian, et al., Carbon 152 (2019) 295–304.
[46] Y. Deng, A.F. Xu, W.T. Wu, et al., New J. Chem. 42 (2018) 7043–7048.
[47] W.J. Gao, Y. Wan, Y.Q. Dou, et al., Adv. Energy Mater. 1 (2011) 115–123.
[48] L.N. Han, X. Wei, Q.C. Zhu, et al., J. Mater. Chem. A 4 (2016) 16698-1605.
[49] C. Gunathilake, R.S. Dassanayake, N. Abidi, et al., J. Mater. Chem. A 4 (2016) 4808–4819.
[50] Z.F. Tian, M.J. Xie, Y. Shen, et al., Chin. Chem. Lett. 28 (2017) 863–867.
[51] W. Luo, Y.H. Li, J. Dong, et al., Angew. Chem. Int. Ed. 125 (2013) 10699–10704.
[52] Y.H. Deng, T. Yu, Y. Wan, et al., J. Am. Chem. Soc. 129 (2007) 1690–1697.
[53] L. Yin, H.B. Wang, L. Li, et al., Appl. Surf. Sci. 476 (2019) 107–114.
[54] D.Y. Fu, C.L. Zhu, X.T. Zhang, et al., J. Mater. Chem. A 4 (2016) 1390–1398.
[55] H. kheel, G.J. Sun, J.K. Lee, et al., Ceram. Int. 42 (2016) 18597–18604.
[56] S. Touba, S. Kimiagar, Mater. Sci. Semicon. Proc. 102 (2019) 104603.
[57] Y.R. Wang, B. Liu, S.H. Xiao, et al., ACS Appl. Mater. Interfaces 8 (2016) 9674–9683.
[58] N.S. Ramgir, C.P. Goyal, P.K. Sharma, et al., Sens. Actuator B: Chem. 188 (2013) 525–532.
[59] H.S. Woo, C.H. Kwak, I.D. Kim, et al., J. Mater. Chem. A 2 (2014) 6412–6418.
[60] N.M. Vuong, D. Kim, H. Kim, Sci. Rep. 5 (2015) 11040.
[61] F.E. Annanouch, Z. Haddi, S. Vallejos, et al., ACS Appl. Mater. Interfaces 7 (2015) 6842–6851.
[62] C.S. Rout, M. Hegde, C.N.R. Rao, Sens. Actuator. B: Chem. 128 (2008) 488–493.
[63] A. Kamalianfar, M.G. Naseri, S.P. Jahromi, Chem. Phys. Lett. 732 (2019) 136648.
[64] V. Najafi, S. Zolghadr, S. Kimiagar, Optik 182 (2019) 249–256.
[65] L.W. Wang, Y.F. Kang, Y. Wang, et al., Mater. Sci. Eng. C 32 (2012) 2079–2085.
[66] H.Y. Jung, Y.L. Kim, S. Park, et al., Analyst 138 (2013) 7206–7211.
[67] S. Keshtkar, A. Rashidi, M. Kooti, et al., Talanta 188 (2018) 531–539.
[68] A. Bagreev, F. Adib, T.J. Bandosz, Carbon 39 (2001) 1897–1905.
[69] T.J. Bandosz, Carbon 37 (1999) 483–491.
[70] V. Meeyoo, D.L. Trimm, N.W. Cant, J. Chem. Technol. Biotechnol. 68 (1997) 411–416.